Supplementary Information (SI) for Journal of Materials Chemistry C.
This journal is © The Royal Society of Chemistry 2025

Supplementary information for

Carrier Lifetime Killer in 4H-SiC: Carrier Capture Path by Carbon Vacancies

Xuanyu Jiang[1,2], Yuanchao Huang[1,2], Rong Wang[1,2], Xiaodong Pi[1,2*], Deren Yang[1,2], and Tianqi Deng[1,2*]

[1]State Key Laboratory of Silicon and Advanced Semiconductor Materials & School of Materials Science and Engineering, Zhejiang University, Hangzhou 310058, China.

[2]Key Laboratory of Power Semiconductor Materials and Devices of Zhejiang Province & Institute of Advanced Semiconductors, ZJU-Hangzhou Global Scientific and Technological Innovation Center, Hangzhou 311215, China.

*Corresponding authors.

E-mail address: dengtq@zju.edu.cn; xdpi@zju.edu.cn.

Part I: Selection of finite volume correction schemes

When using periodic boundary conditions in DFT, the total energy of charged defect is actually obtained from a supercell embedded a compensating background charge and contaminated by long-ranged Coulomb interactions. Though the supercell we adopted is quite large, a correction of finite volume is still necessary. Several processing methods have been proposed to modified this problem. However, a systematic understanding of the performance and applicability of these schemes for 4H-SiC is still lacking. Here we compare the most popular method introduced by Freysoldt, Neugebauer, and Van de Walle (FNV method)[1] with the method generalized by Kumagai, and Oba (eFNV method)[2] on the purpose to assess the impact to 4H-SiC brought by the finite volume in periodic boundary conditions.

The correction energy of the FNV scheme in charge state q can be expressed as:

$$E_{FNV} = E_{PC} - q\Delta V_{PC,q/b}|_{far} \tag{1}$$

where E_{PC} is a point charge correction, $\Delta V_{PC,q/b}$ is the potential difference between the PC potential $V_{PC,q}$ and the planar-averaged defect-induced potential $V_{q/b} = V_{defect,q} - V_{bulk}$. The $\Delta V_{PC,q/b}|_{far}$ is $\Delta V_{PC,q/b}$ farthest from the defect center in supercell and often called as potential alignment term which can couple to the unscreened or partially screened charge distribution beyond the PC correction even the details of the screening are unknown. However, the farthest atomic site from the defect is not always the best reference for evaluating potential alignment term. This is because there might be non-negligible overlap of defect wave functions existing in the farthest atomic site lying between the defect and its periodic images. Therefore, a method of replacing the $\Delta V_{PC,q/b}|_{far}$ with an average $\Delta V_{PC,q/b}$ is proposed. The sampling region of the average potential alignment term locates outside the Wigner-Seiz cell with radius R_{WS} which does not depend on the choice of the supercell. Also in this way, the FNV method which is only suitable for isotropic materials has been generalized as the eFNV method that can be applied to anisotropic systems.

The correction energies of V_C comparing the FNV and eFNV methods are partly illustrated in Supplementary Figure 1 to Supplementary Figure 4. Because the dielectric

tensors of 4H-SiC have different diagonal components, the isotropic FNV correction with a dielectric constant, which is a typical approximation, does not avail to correct the total energy of charged defect in 4H-SiC. On the other hand, the anisotropic eFNV method can not only get the potential alignment inside R_{WS} but also correct the shape dependence of supercell. Thus, the eFNV method is adopted in this work.

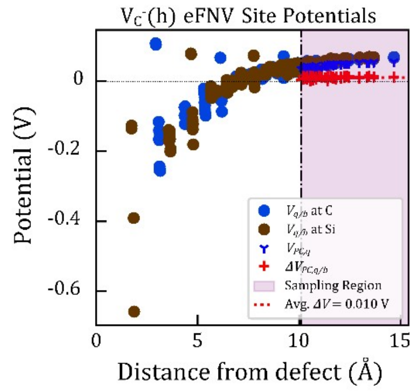

Supplementary Figure 1 Illustration of planar-averaged defect-induced potential $V_{q/b}$ at different C and Si atoms in supercell, PC potential $V_{PC,q}$,and their difference $\Delta V_{PC,q/b}$ at sampling region of $V_C^-(h)$ using the eFNV method.

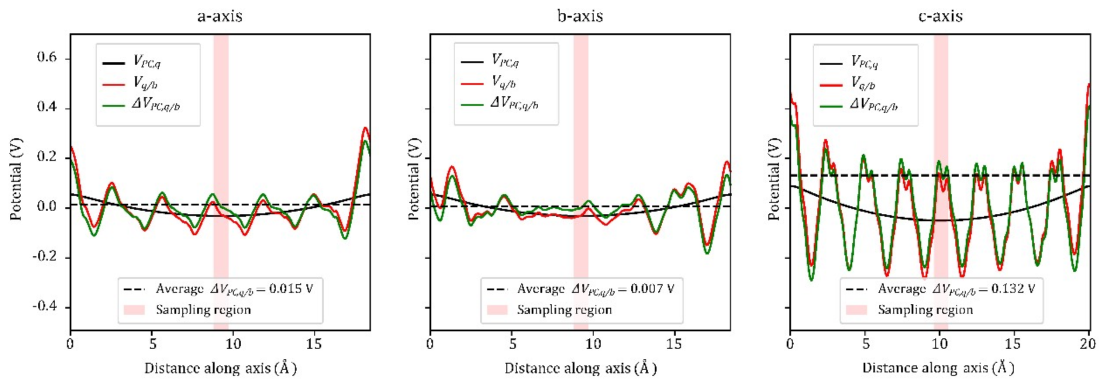

Supplementary Figure 2 Illustration of PC potential $V_{PC,q}$, planar-averaged defect-induced potential $V_{q/b}$, and their difference $\Delta V_{PC,q/b}$ at sampling region of $V_C^-(h)$ along the a-axis, b-axis, and c-axis using the FNV method.

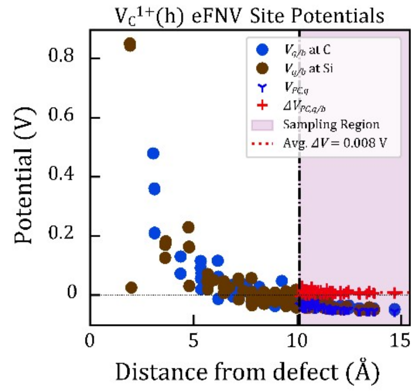

Supplementary Figure 3 Illustration of planar-averaged defect-induced potential $V_{q/b}$ at different C and Si atoms in supercell, PC potential $V_{PC,q}$,and their difference $\Delta V_{PC,q/b}$ at sampling region of $V_C^+(h)$ using the eFNV method.

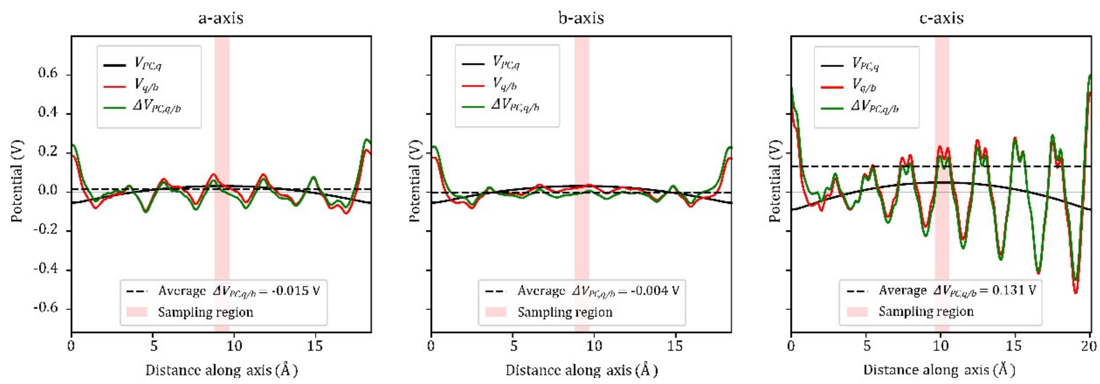

Supplementary Figure 4 Illustration of PC potential $V_{PC,q}$, planar-averaged defect-induced potential $V_{q/b}$, and their difference $\Delta V_{PC,q/b}$ at sampling region of $V_C^+(h)$ along the a-axis, b-axis, and c-axis using the FNV method.

Part II: The results of 1D configuration coordinate diagram and nonradiative carrier capture sections

This part includes: Supplementary Figure 5 to Supplementary Figure 12

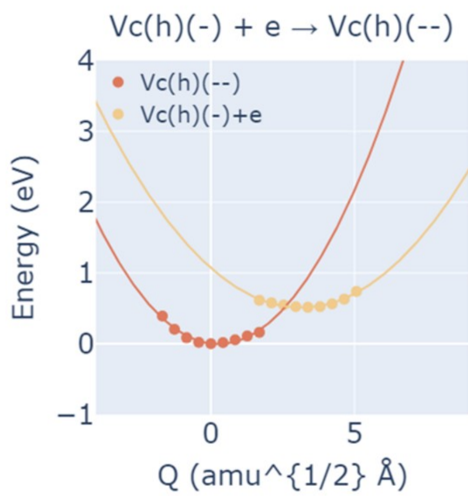

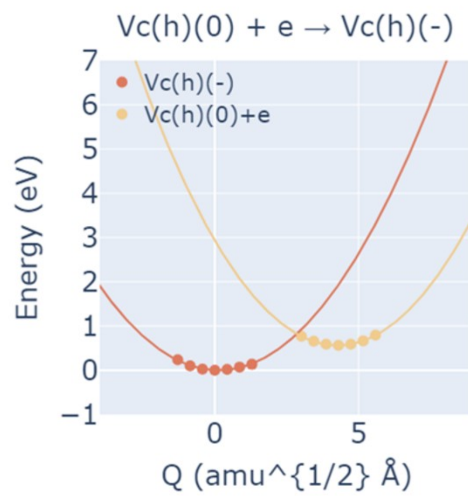

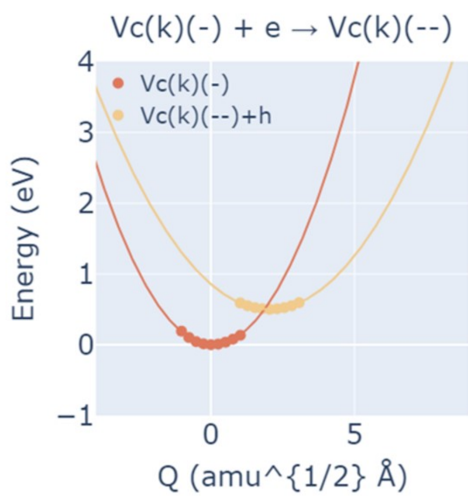

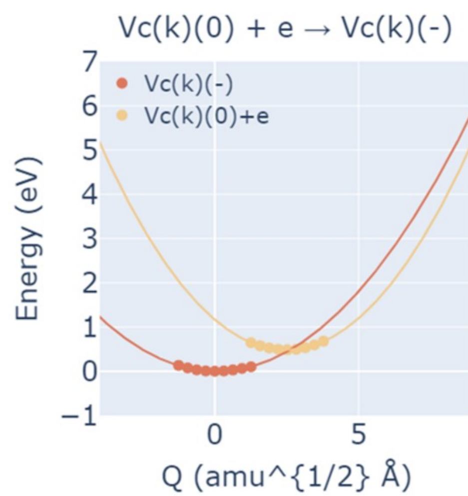

Supplementary Figure 5 Calculated 1D configuration coordinate diagram for electron capture at the acceptor levels of V_C defect in 4H-SiC. Symbols: calculated values; solid line: parabolic fit.

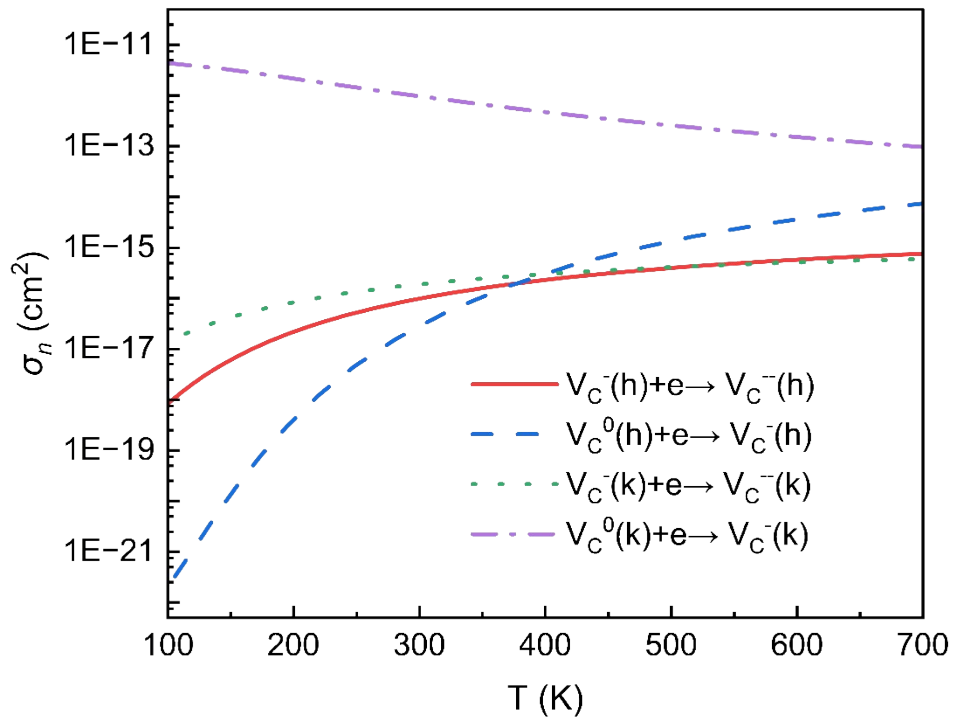

Supplementary Figure 6 Nonradiative electron capture section for electron capture at the acceptor levels of V_C defect in 4H-SiC.

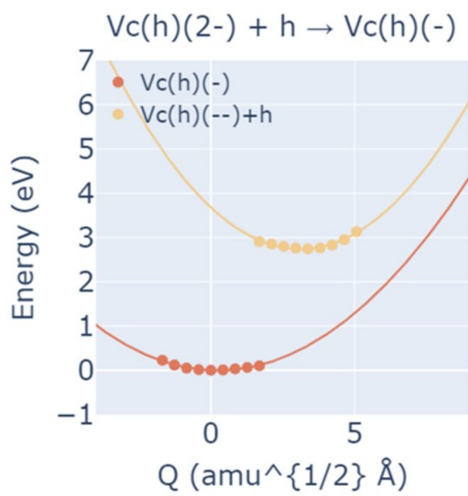

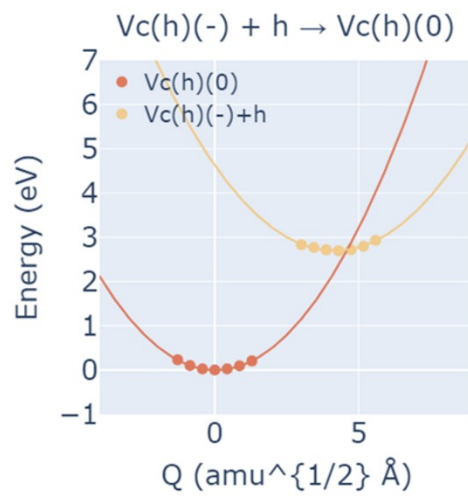

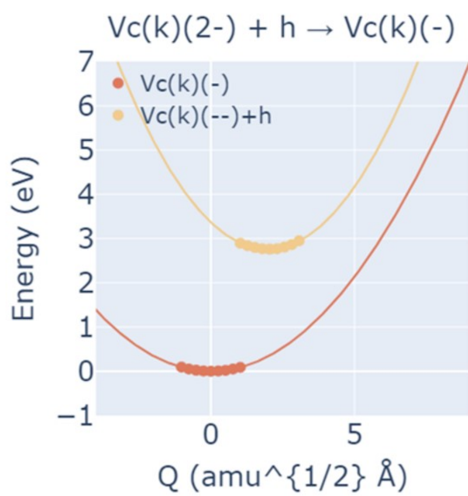

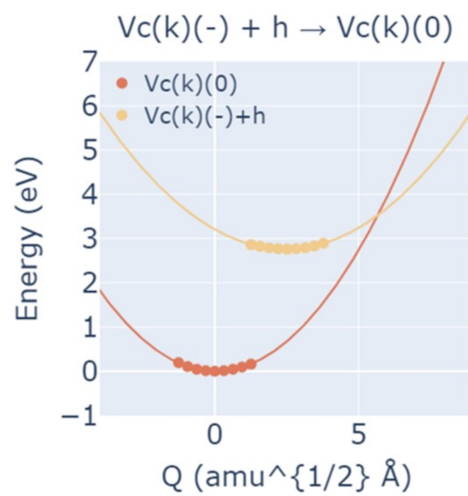

Supplementary Figure 7 Calculated 1D configuration coordinate diagram for hole capture at the acceptor levels V_C defect in 4H-SiC. Symbols: calculated values; solid line: parabolic fit.

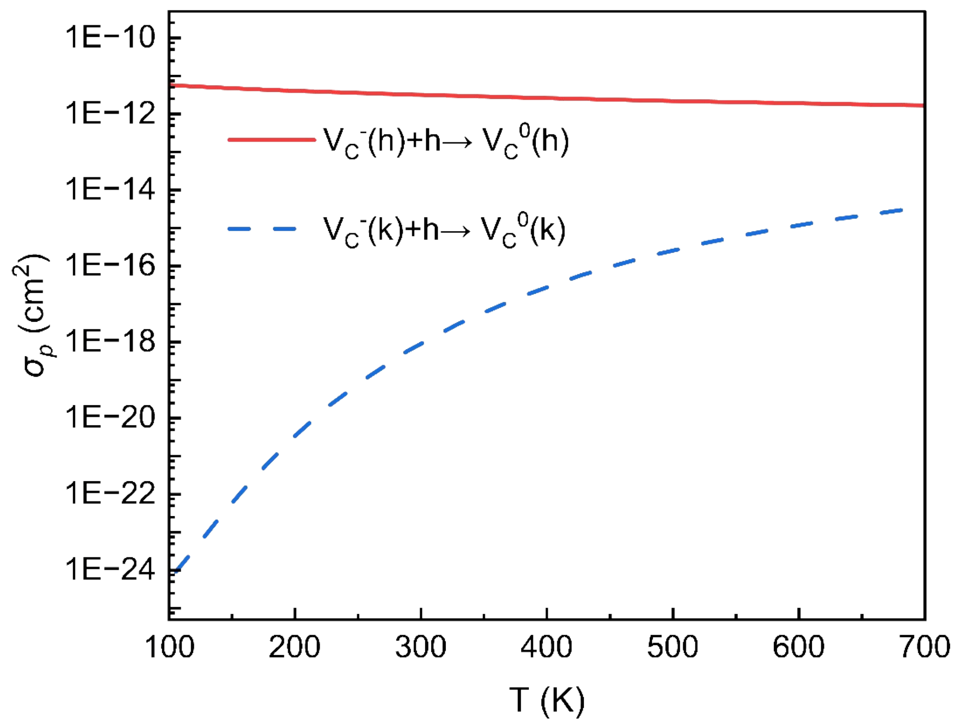

Supplementary Figure 8 Nonradiative hole capture section for hole capture at the acceptor levels V_C defect in 4H-SiC.

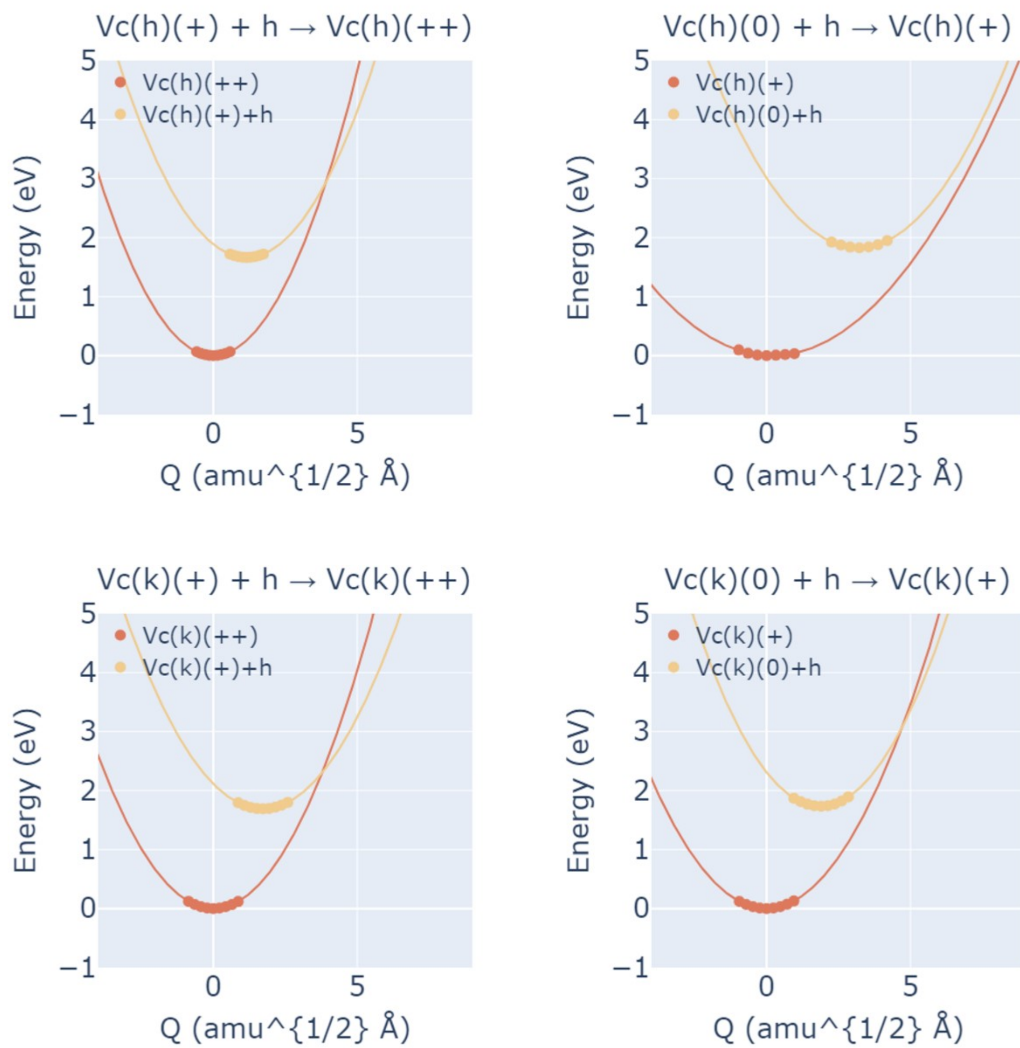

Supplementary Figure 9 Calculated 1D configuration coordinate diagram for hole capture at the donor levels of V_C defect in 4H-SiC. Symbols: calculated values; solid line: parabolic fit.

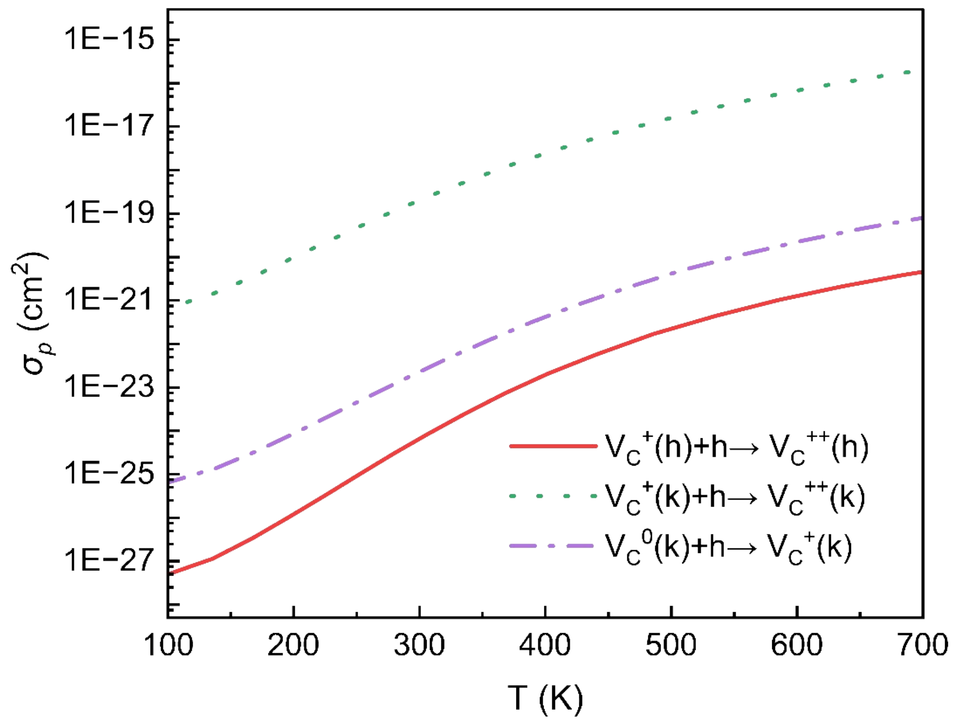

Supplementary Figure 10 Nonradiative electron capture section for hole capture at the donor levels of V_C defect in 4H-SiC.

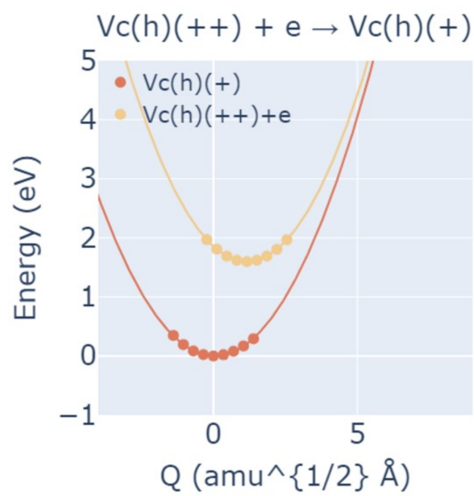

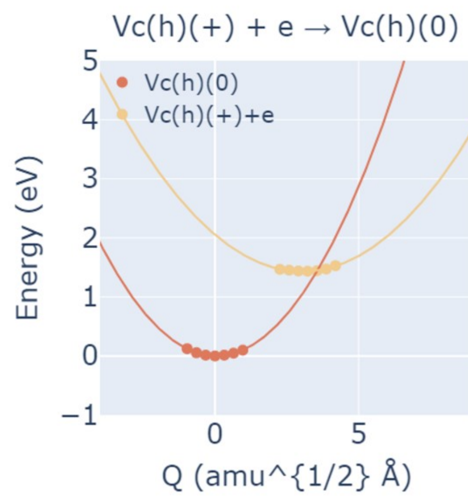

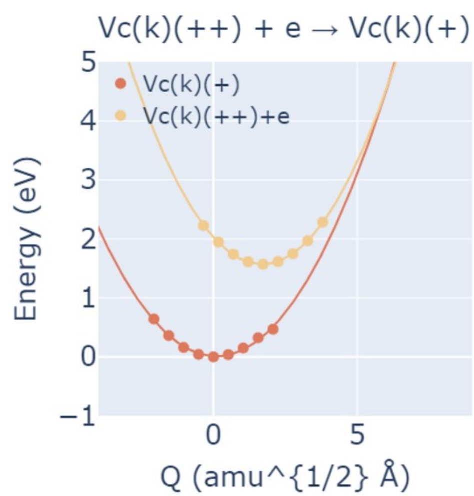

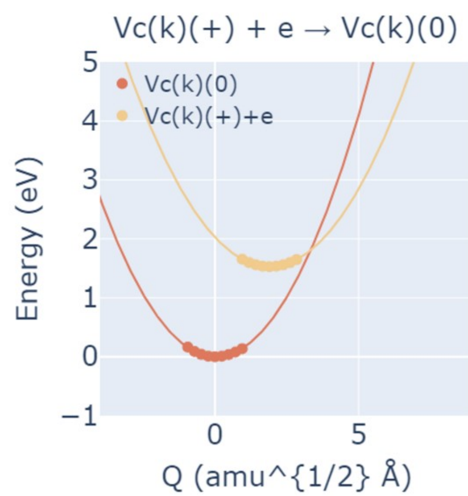

Supplementary Figure 11 Calculated 1D configuration coordinate diagram for electron capture at the honor levels V_C defect in 4H-SiC. Symbols: calculated values; solid line: parabolic fit.

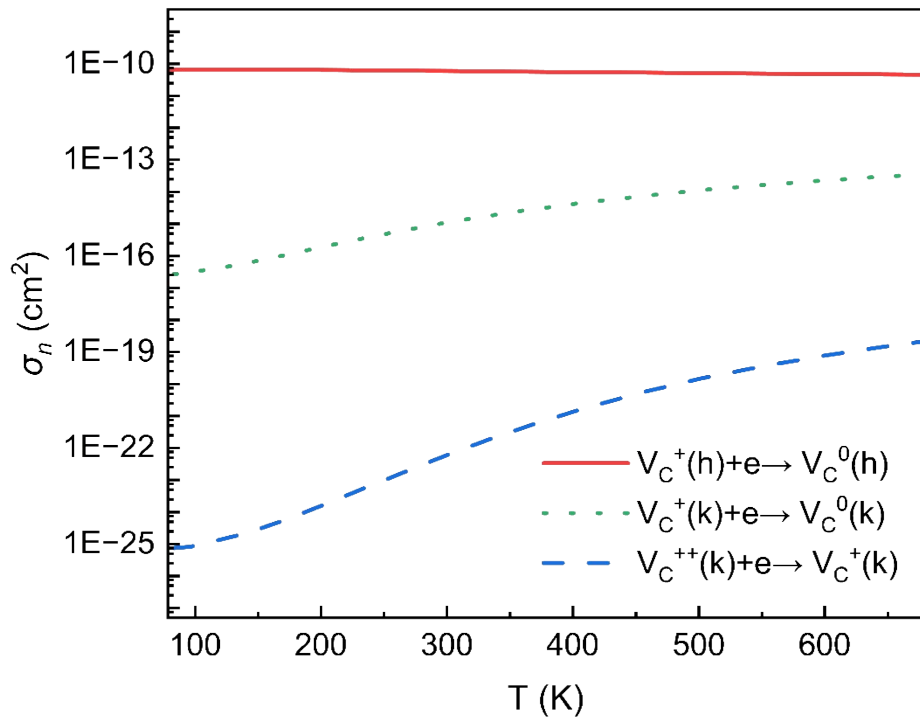

Supplementary Figure 12 Nonradiative hole capture section for electron capture at the donor levels V_C defect in 4H-SiC.

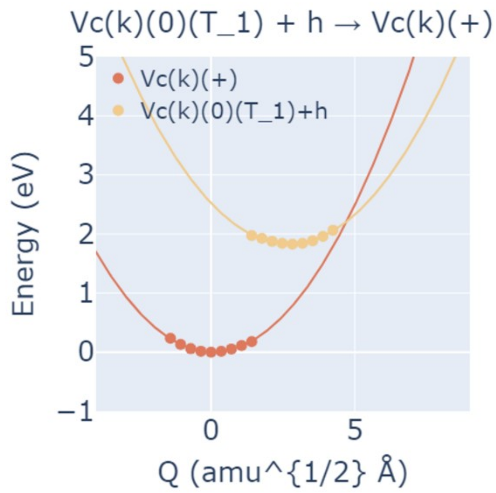

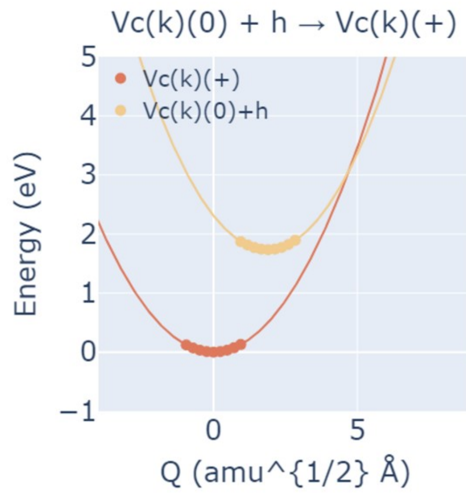

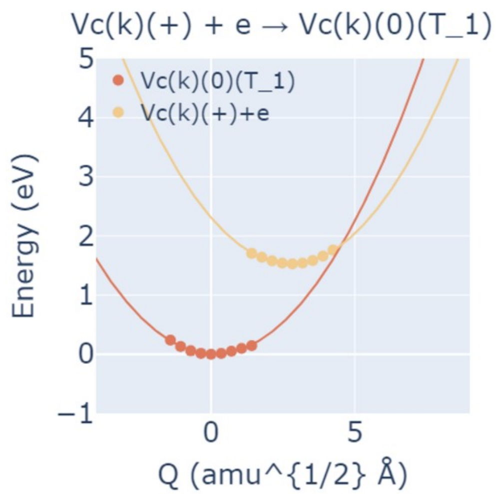

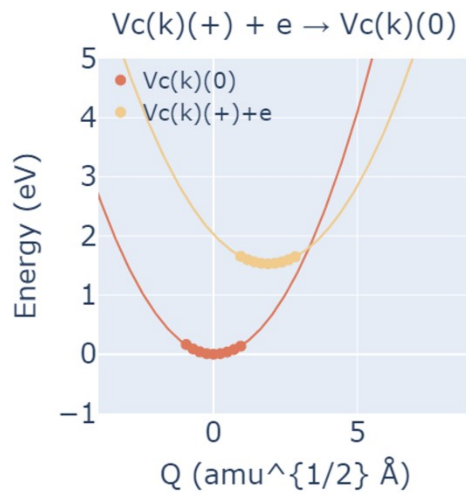

Supplementary Figure 12 Calculated 1D configuration coordinate diagram for hole capture at the neutral triplet and singlet state V_C(k) defect, as well as for electron capture at the positive charge state V_C(k) defect and thus becoming neutral triplet and singlet state V_C(k) in 4H-SiC. Symbols: calculated values; solid line: parabolic fit.

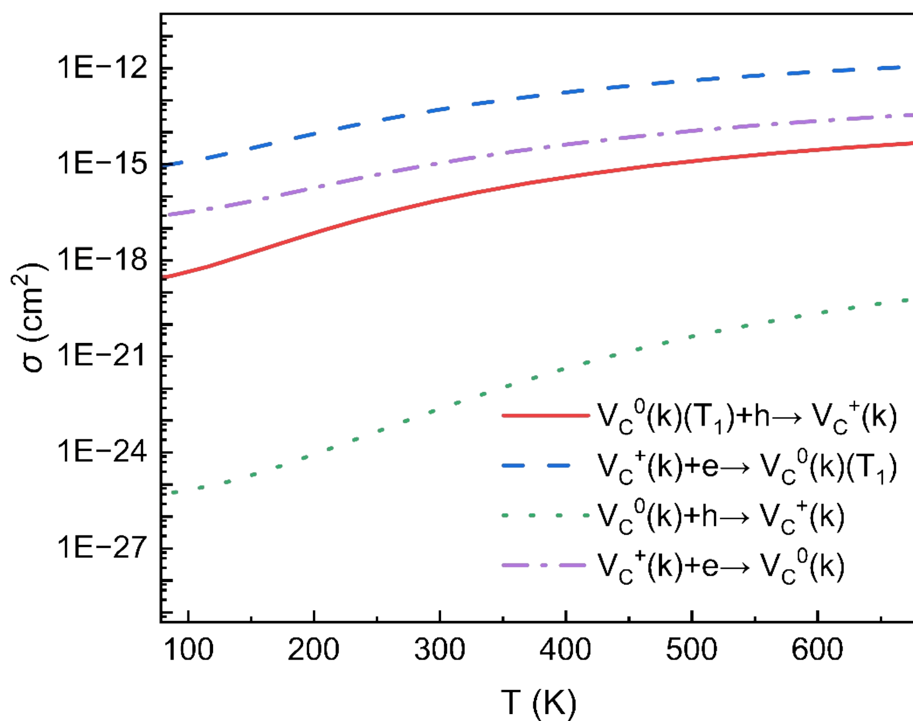

Supplementary Figure 14 Nonradiative hole capture section at the V_C(k) defect from neutral triplet and singlet state to positive charge state, as well as nonradiative electron capture section form positive charge state to neutral triplet and singlet state in 4H-SiC as a function of temperature.

Part III: Detail for the relaxed structure

This part includes: Supplementary Table 1, Supplementary Table 2 and Supplementary Figure 15 to Supplementary Figure 18.

Supplementary Table 1 Structure details for the $V_C(h)$ and $V_C(k)$ in 4H -SiC at different charge states (−2≤q≤+2). Structures are specified by the distance between the neighbor Si atoms variations, symmetry, configuration belonging to, and the total energy difference between initial and final structure.

		$Si_{\perp BP} - Si_{\parallel BP}$ (Å)			$Si_{\parallel BP} - Si'_{\parallel BP}$ (Å)			Symmetry, Configuration	ΔE
With Disturbance and Low-spin State	$V^{2-}_C(h)$	4.73%	-11.82%	4.73%	-16.16%	4.49%	-16.24%	C_s,D	33.90
	$V^{-}_C(h)$	2.06%	1.89%	0.03%	-13.76%	0.95%	0.71%	C_s,C	24.03
	$V_C(h)$	-6.65%	5.87%	5.87%	4.16%	4.02%	-7.60%	C_s,B	14.04
	$V^{+}_C(h)$	8.74%	8.88%	8.71%	5.14%	5.00%	5.00%	C_{3v},A	4.62
	$V^{2+}_C(h)$	10.53%	10.53%	10.53%	10.04%	9.89%	9.89%	C_{3v},A	-4.86
	$V^{2-}_C(k)$	3.92%	-15.70%	3.92%	-15.45%	4.29%	-15.56%	C_s,D	33.86
	$V^{-}_C(k)$	5.44%	-14.15%	5.44%	-5.44%	1.32%	-5.54%	C_s,D	24.00
	$V_C(k)$	5.87%	-8.37%	5.87%	4.60%	-6.79%	4.46%	C_s,B	13.92
	$V^{+}_C(k)$	8.54%	1.86%	8.58%	6.86%	2.36%	6.72%	C_s,B	4.58
	$V^{2+}_C(k)$	11.78%	11.78%	11.78%	9.80%	9.66%	9.66%	C_{3v},A	-4.91
Without Disturbance nor Low-spin State	$V^{2-}_C(h)$	0.14%	0.24%	0.14%	-7.74%	-7.93%	-7.87%	C_{3v},A	34.37
	$V^{-}_C(h)$	-0.17%	-0.14%	-0.17%	-2.43%	-2.57%	-2.57%	C_{3v},A	24.39
	$V_C(h)$	2.36%	6.41%	5.81%	-2.54%	-4.29%	6.28%	C_s,D	14.32
	$V^{+}_C(h)$	8.74%	8.85%	8.71%	5.14%	5.00%	5.00%	C_{3v},A	4.62
	$V^{2+}_C(h)$	10.53%	10.53%	10.53%	10.04%	9.89%	9.89%	C_{3v},A	-4.86
	$V^{2-}_C(k)$	-2.26%	-2.26%	-2.26%	-0.91%	-1.05%	-1.05%	C_{3v},A	34.40
	$V^{-}_C(k)$	-2.16%	-2.16%	-2.16%	-0.88%	-1.01%	-1.01%	C_{3v},A	24.22
	$V_C(k)$	0.95%	4.56%	4.52%	-4.23%	4.49%	1.22%	C_s,C	14.29
	$V^{+}_C(k)$	4.56%	4.76%	0.71%	1.76%	-4.69%	4.29%	C_s,C	6.19
	$V^{2+}_C(k)$	11.78%	11.78%	11.78%	9.80%	9.66%	9.66%	C_{3v},A	-4.91

Supplementary Table 2 Magnetic moment, spin state, symmetry, and structure configuration details for $V_C(h)$ and $V_C(k)$ in 4H-SiC at different charge states (−2≤q≤+2)

Defect	Magnetic Moment	Spin State	Symmetry, Configuration
$V^{2-}_{C}(h,D)$	0.0	singlet	C_s,D
$V^{-}_{C}(h,C)$	1.0	doublet	C_s,C
$V_C(h,B)$	0.0	singlet	C_s,B
$V^{+}_{C}(h,A)$	1.0	doublet	C_{3v},A
$V^{2+}_{C}(h,A)$	0.0	singlet	C_{3v},A
$V^{2-}_{C}(k,D)$	0.0	singlet	C_s,D
$V^{-}_{C}(k,D)$	1.0	doublet	C_s,D
$V_C(k,B)$	0.0	singlet	C_s,B
$V_C(k,A)$	2.0	triplet	C_{3v},A
$V^{+}_{C}(k,B)$	1.0	doublet	C_s,B
$V^{2+}_{C}(k,A)$	0.0	singlet	C_{3v},A

NVT molecular dynamics simulations are performed for carbon vacancies to validate the stability of the defect structures. The results are presented in Supplementary Figures 15 to Supplementary Figures 18. The four nearest-neighbor Si atoms to the carbon vacancy were selected as candidates and are denoted as Si1, Si2, Si3, and Si4. Among these, Si2, Si3, and Si4 lie within the basal plane, while Si1 is positioned along the direction perpendicular to the basal plane. As shown in Supplementary Figures 15 to Supplementary Figures 18, the Si atoms surrounding the defect vibrate with similar amplitudes, and no significant structural changes or vacancy migration are observed in the defect region. This observation indicates that the defect structures remain stable throughout the simulation, which further validates the methodology used in this study to obtain stable defect configurations.

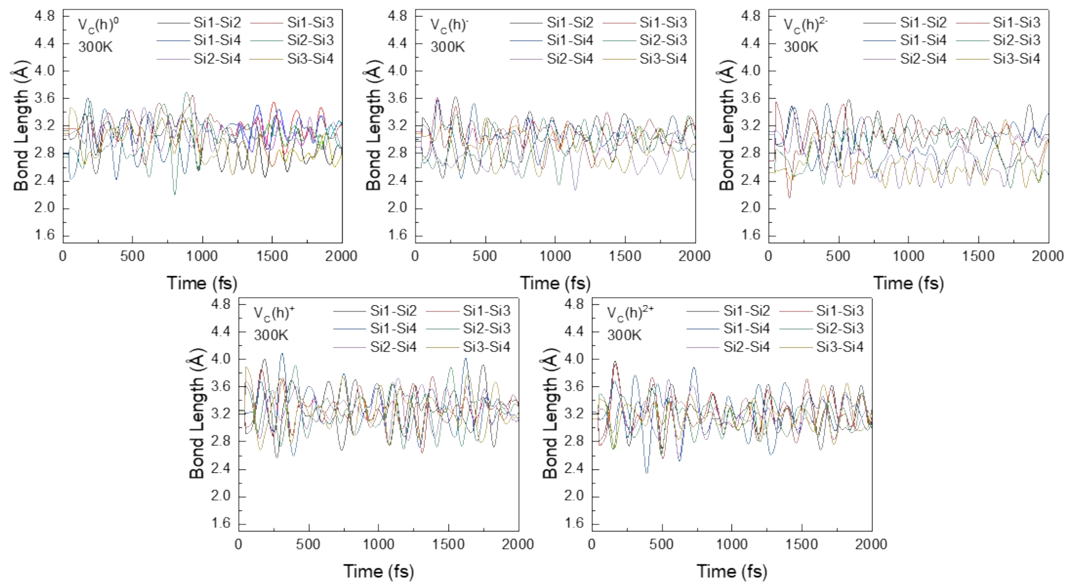

Supplementary Figure 15 Room temperature (300 K) NVT trial for $V_C(h)$ at different charge states (−2≤q≤+2)

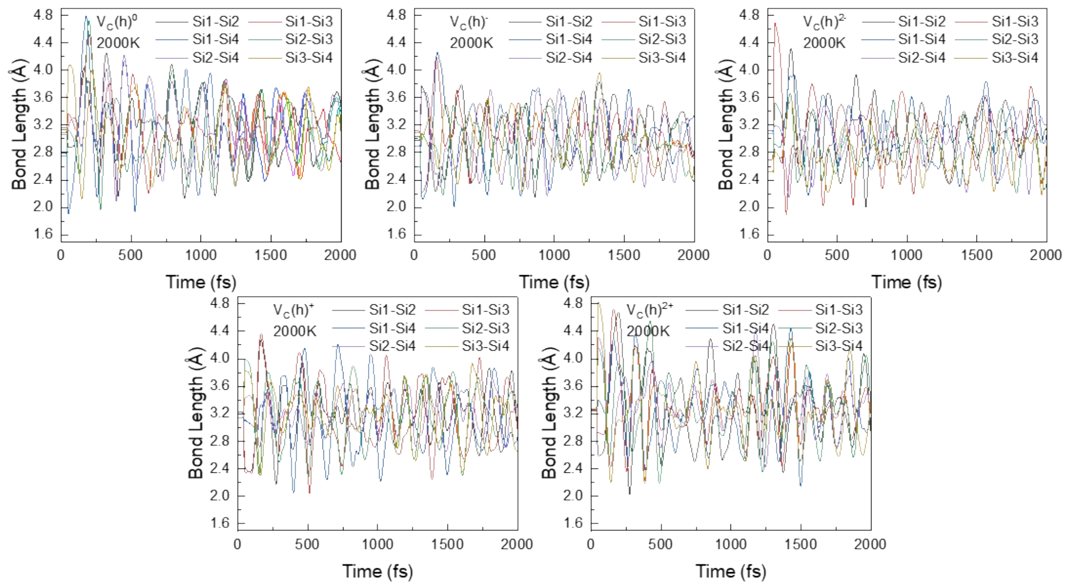

Supplementary Figure 16 High temperature (2000 K) NVT trial for $V_C(h)$ at different charge states (−2≤q≤+2)

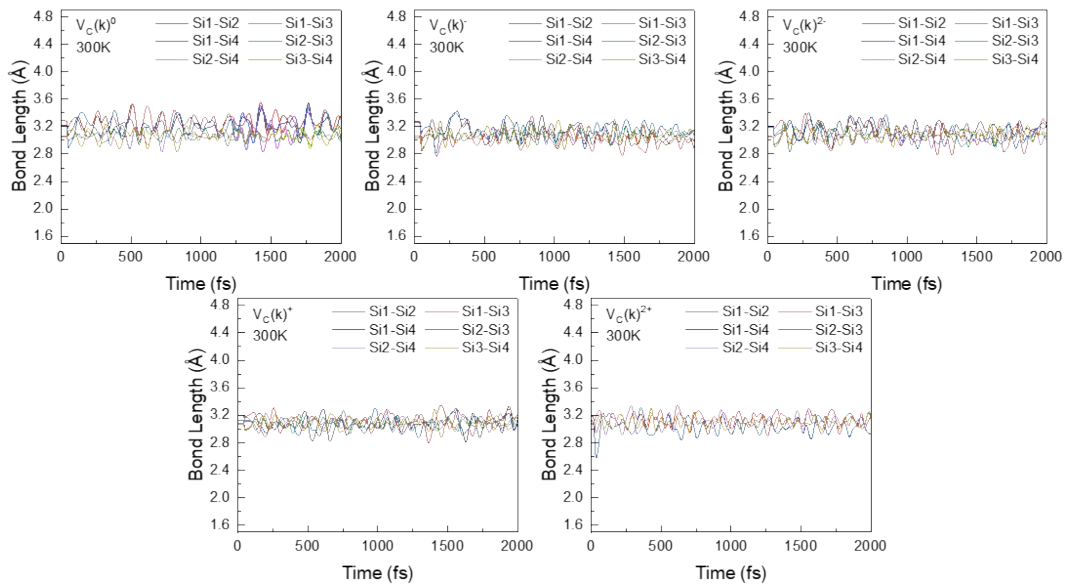

Supplementary Figure 17 Room temperature (300 K) NVT trial for $V_C(k)$ at different charge states (−2≤q≤+2)

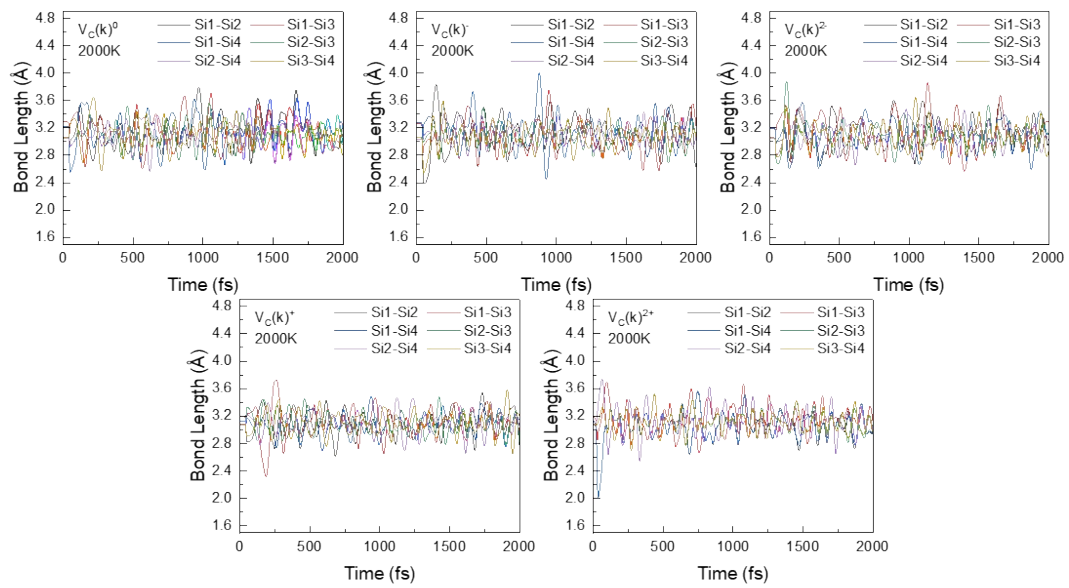

Supplementary Figure 18 High temperature (2000 K) NVT trial for $V_C(k)$ at different charge states ($-2 \leq q \leq +2$)

Reference

1 Freysoldt, C., Neugebauer, J. & Van de Walle, C. G. Fully Ab Initio Finite-Size Corrections for Charged-Defect Supercell Calculations. Physical Review Letters 102, 016402 (2009). https://doi.org:10.1103/PhysRevLett.102.016402

2 Kumagai, Y. & Oba, F. Electrostatics-based finite-size corrections for first-principles point defect calculations. Physical Review B 89, 195205 (2014). https://doi.org:10.1103/PhysRevB.89.195205